STUDY OF $J/\psi \to \phi K_s K_s$ IN BESIII EXPERIMENT

by

Engin Eren

B.S., Physics, Boğaziçi University, 2013

Submitted to the Institute for Graduate Studies in
Science and Engineering in partial fulfillment of
the requirements for the degree of
Master of Science

Graduate Program in Physics

Boğaziçi University

2015

ACKNOWLEDGEMENTS

It would be very hard to perfom my analysis without the help of our group members. That is why I would like to thank my co-advisor Ismail Uman and and my supervisor Erkcan Ozcan along with Ph.D. student Onur Kolcu and Master student Alperen Yuncu. Additionaly, I would like to thank Serkant Ali Cetin and Gokhan Unel for their external support for our analysis and to my family who motivated me until the last moment.

ABSTRACT

STUDY OF $J/\psi \to \phi K_s K_s$ IN BESIII EXPERIMENT

In this thesis, 1.3 billion of J/ψ events collected by Beijing Electron Spectrometer (BES) III experiment have been analyzed. The decay channel of J/ψ meson, $J/\psi \to \phi K_s K_s$, has been studied and the Dalitz plot has been produced. In the $K_s K_s$ invariant mass distribution, two peaks one at ~ 1 GeV, and one at ~ 1.5 GeV, which correspond presumably to the tetra-quark candidate $f_0(980)$, $f_2'(1525)$ and/or glueball candidate $f_0(1500)$, respectively, has been observed. Another shoulder at 1.7 GeV has been observed and it is hypothesized to be $f_0(1710)$. Background studies showed that this channel is very selective and can be used to perform a detailed partial wave analysis, which will serve to confirm the results from earlier BESII data.

ÖZET

BESIII DENEYİNDE $J/\psi \to \phi K_s K_s$ ÇALIŞMASI

Bu tezde Beijing Elektron Pozitron Spektrometresi III (BESIII) deneyi tarafından toplanan 1.3 milyar J/ψ olayı incelenmiştir. J/ψ mezonunun özel bir bozunum kanalı olan $J/\psi \to \phi K_s K_s$ çalışılmıştır ve Dalitz grafiği elde edilmiştir. $K_s K_s$ değişmez kütle dağılmında iki tane tepe ve bir tane de tepecik görülmüştür. 1 GeV civarı olan tepenin dörtlü-quark adayı $f_0(980)$, diğer tepenin ise glutopu adayı $f_0(1500)$ (veya $f_2'(1525)$) olduğu düşünülmektedir. Tepecik ise $f_0(1710)$ rezonansı adayıdır. Çalışmamız gösteriyor ki bozunum kanalımız hafif kuark meson ve rezonanslarına kısmi dalga analizi yapmak için ideal bir adaydır. BESII deneyinde araştırılan $J/\psi \to \phi K^+ K^-$ kanalına göre daha az ardalan içerir ve veri istatistiği daha yüksektir. Gerçek veri ve benzetim verisi kullanılarak ardalan katkısı hesaplanmıştır.

TABLE OF CONTENTS

LIST OF FIGURES

LIST OF TABLES

LIST OF ACRONYMS/ABBREVIATIONS

BESII	Beijing Electron Spectrometer II
BESIII	Beijing Electron Spectrometer III
MC	Monte Carlo
PWA	Partial Wave Analysis
PID	Particle Identification
QCD	Quantum Chromodynamics

1. INTRODUCTION

1.1. Quantum Chromodynamics

To explain the binding of protons and neutrons in the atomic nucleus after neutron's discovery, a new fundamental force, the strong force, was postulated. After the successful theory of quantum electrodynamics (QED), a relativistic formulation of the quantum theory of strong interaction, called quantum chromodynamics (QCD), was proposed. According to QCD, baryons consist of three quarks, whereas mesons consist of quark-antiquark pairs. Quarks and anti-quarks have spin 1/2. The quarks exist to be in several forms called "flavour". Flavours are labeled as u, d, s, c, b and t, which stands for up, down, strange, charm, bottom (beauty), and top. The quark content of the proton is uud and of the neutron is udd. To account for the charge of proton and neutron, the u and d quarks are assigned to have charges 2/3 and -1/3, respectively. The light charged pseudoscalar mesons such as π^+ and π^- have quark content $u\bar{d}$ and $d\bar{u}$, while the neutral π^0 is a linear combination of $u\bar{u}$ and $d\bar{d}$. Moreover, strange pseudoscalar mesons like K^+ and K^0 have quark content $u\bar{s}$ and $d\bar{s}$. To be consistent with the Pauli exclusion principle, Han and Nambu, Greenberg and Gell-Mann, proposed to add an additional degree of freedom, the "color charge" [5,6]. With the color, the baryon wave-function becomes anti-symmetric under the interchange of any two quarks. With three flavors u, d and s, and three colors, it is possible to construct multiplets that form irreducible representation of SU(3). For baryons, the combinations decompose into a decouplet, a singlet and two octets according to the rule

$$3 \otimes 3 \otimes 3 = 10 \oplus 8 \oplus 8 \oplus 1. \tag{1.1}$$

For mesons, we obtain an octet and a singlet

$$3 \otimes \overline{3} = 8 \oplus 1. \tag{1.2}$$

Using the spectroscopic notation a $q\overline{q}$ state is written as $n^{2S+1}L_J$, where n is the radial quantum number, L is the orbital angular momentum, S is the total spin and J is the total angular momentum. For L we use the letter convention as in atomic physics with S,P,D for $L = 0, 1, ...$ For fermion-anti fermion, parity operator is $P = (-1)^{L+1}$; and C parity is $C = (-1)^{L+S}$. For pseudoscalar mesons with $L = 0$ (ground state), $J^{PC} = 0^{-+}$, whereas for vector mesons (with $L = 0$) $J^{PC} = 1^{--}$. As an example in the quark model assignment, lowest-lying pseudoscalar and vector meson nonets are

$$
\begin{aligned}
1^1S_0 \;&\rightarrow\; \pi(140), \eta(547), K(495), \eta'(958) \\
1^3S_1 \;&\rightarrow\; \rho(770), \omega(782), \phi(1020), K^*(892)
\end{aligned}
$$

and the octet and singlet (nonet) are represented in Figure 1.1.

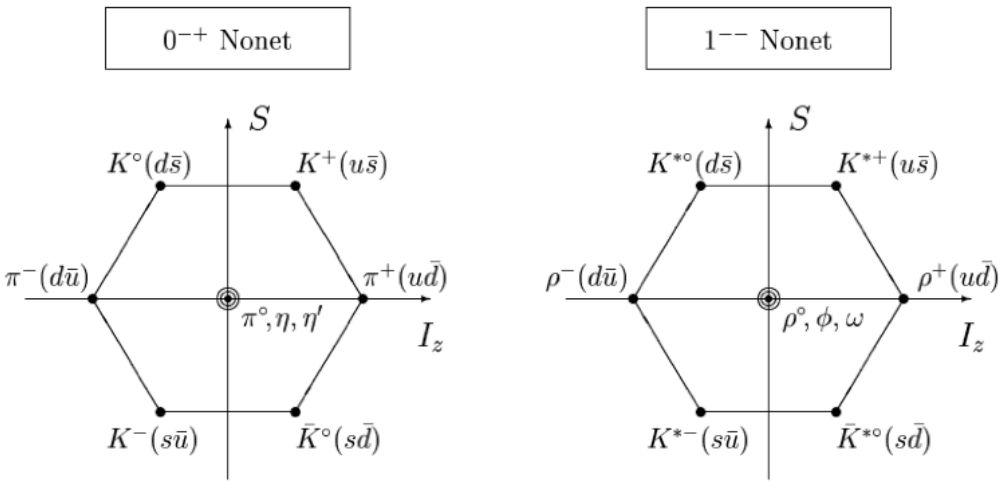

Figure 1.1. Representation of the lowest-lying meson states with their respective quark assignments. $\pi^0, \rho : (u\overline{u} - d\overline{d})/\sqrt{2}$ and $\eta, \eta', \omega, \phi : c_1(s\overline{s}) + c_2(n\overline{n})$, where $n\overline{n} = (u\overline{u} \pm d\overline{d})/\sqrt{2})$ [1].

1.2. Glueballs and Tetraquarks

According to QCD, strong force is carried out by spin-1 particles, named "gluons". Since gluons carry color charge, they can also attract each other in additon to interact

with quarks. Therefore, there could be a new form of matter like *glueballs*, states of two or three gluons (gg or ggg) and *hybrids* ($q\bar{q}g$). The study of such states from first principle is difficult, due to the non-perturbative nature of QCD at low energy scales. Lattice QCD is a formulation of the quark-gluon interaction on a space-time lattice. Quenched (without quarks) lattice QCD simulations suggest that the lightest scalar glueball ($J^{PC} = 0^{++}$) is the lightest of these states, with a mass in the $1.5 \sim 1.7$ GeV range. In addition, lattice QCD predicts the presence of a tensor glueball, having $J^{PC} = 2^{++}$ quantum numbers, with a mass around 2300 MeV [7, 8]. The predictions based on the QCD Sum Rules tecnique for the value of the scalar glueball mass, having $J^{PC} = 0^{++}$ quantum numbers, is lower, it somewhat should lie around 1250 MeV [9].

Glueballs are predicted to have no flavour and they are electrically neutral. Therefore, it is expected that they do not have a preferred decay to a particular quark flavour or charge. A flavour singlet, like a glueball, has zero isospin. The scalar glueball candidate could decay in an S channel into a pairs of pseudoscalars such as $\pi\pi, K_s\,K_s, K^+K^-, \eta\eta$ [10]. For flavor blind decay, we expect that the glueball candidate decay with the following branching fractions:

$$\frac{\Gamma(G \to \pi\pi, K\overline{K}, \eta\eta, \eta\eta', \eta'\eta')}{Phase\ Space} = 3 : 4 : 1 : 0 : 1 \tag{1.3}$$

The fact that glueballs have the same quantum numbers as $q\bar{q}$ mesons complicates their identification. For the scalar nonet we have too many f_0 mesons with mass greater than 1 GeV in the relevant range : $f_0(1370)$, $f_0(1500)$ and $f_0(1710)$. One of them could be the bare glueball state or according to the mixing scheme, a physical resonance $f_0(m_i)$ can be decomposed as [7, 11] :

$$f = \alpha\,|n\overline{n}\rangle + \beta\,|s\bar{s}\rangle + \gamma\,|G\rangle + \delta\,|q\bar{q}q\bar{q}\rangle \tag{1.4}$$

Here $|n\overline{n}\rangle$ stands for non-strange (u and d) quark content, $|s\bar{s}\rangle$ is for strange quark content, $|G\rangle$ and $|q\bar{q}q\bar{q}\rangle$ stand for glueball and tetra-quark contributions, respectively. This means that the already observed resonances can have glueball and/or tetra-quark

contributions. Therefore, careful understanding of conventional $q\bar{q}$ mesons is fundamental.

In BESIII experiment, charmonium decays are gluon rich decay processes where glueballs can be produced. We can distinguish J/ψ decays in radiative and hadronic decay channels. Feynman diagrams for glueball production via radiative and hadronic decays of J/ψ are represented in Figure 1.2.

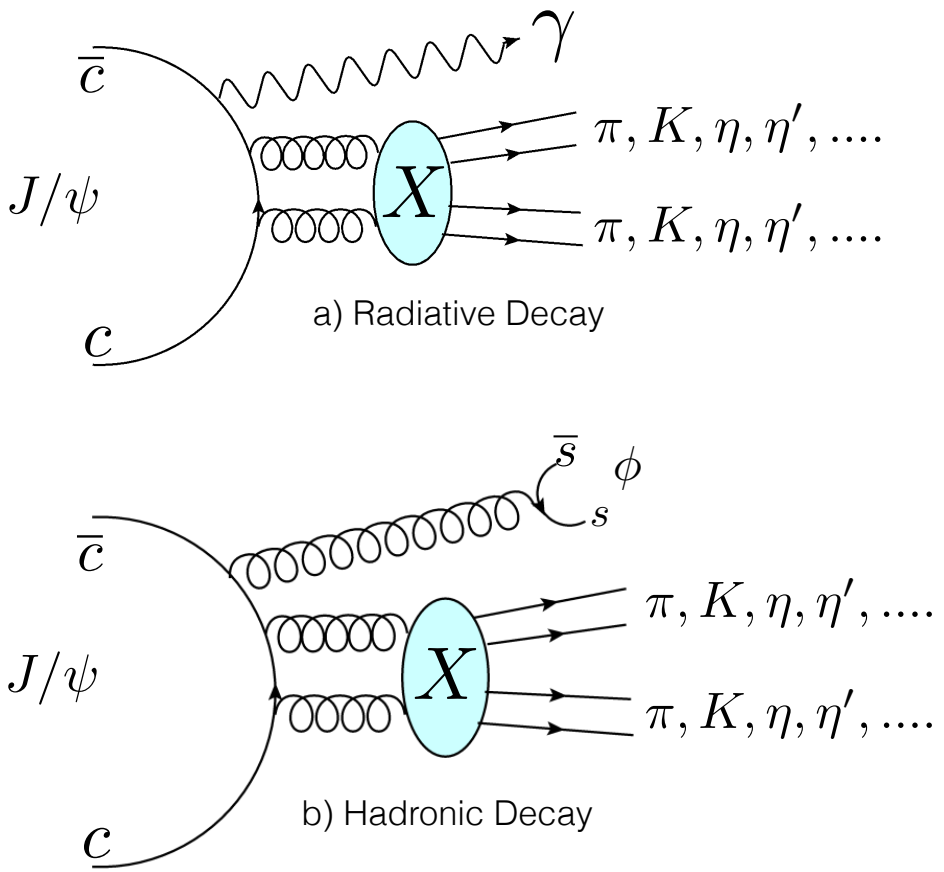

Figure 1.2. Glueball production via (a) radiative and (b) hadronic decay of J/ψ. X stands for a glueball.

1.3. Scalar Glueball Candidates

As mentioned earlier, there are too many isoscalar scalar ($I^G J^{PC} \equiv 0^+0^{++}$, where G is G-partiy defined as $G = (-1)^{l+s+I}$) states in the 1$\sim$2 GeV mass region: $f_0(1370)$, $f_0(1500)$ and $f_0(1710)$. In this subsection, we review the earlier experimental data on

these scalar glueball candidates.

1.3.1. The $f_0(1370)$

Crystal Barrel experiment observed $f_0(1370)$ via its decay mode $f_0(1370) \to K\overline{K}$ [12]. WA102 proton-proton scattering experiment confirmed this resonance in the $\pi\pi$, $K\overline{K}$ and $\eta\eta$ decay channels [13]. The $f_0(1370)$ is likely to be a candidate for a $n\overline{n}$ scalar meson ($n = u$ or d) due to the large value of the ratio [13] :

$$\frac{BR_{f_0(1370)\to\pi\pi}}{BR_{f_0(1370)\to K\overline{K}}} = 2.17 \pm 0.9 \tag{1.5}$$

According to the results of BESII experiment, a $f_0(1370)$ signal is present in $J/\psi \to \phi\pi^+\pi^-$ [4]. The partial wave analysis (PWA) in this channel shows that the peak around 1370 MeV stems from a dominant $f_0(1370)$ term that interferes with the nearby $f_2(1270)$ and $f_0(1500)$.

1.3.2. The $f_0(1500)$

Most of the knowledge about $f_0(1500)$ comes from the Crystal Barrel collaboration. They resolved two scalar states in this mass region and determined their decay branching ratios to a number of final states like $\pi^0\pi^0$, $\eta\eta$, $\eta\eta'$, K_LK_L and $4\pi^0$ [8, 14]. This, together with the fact that $f_0(1500)$ is absent in glueball suppressed processes such as $\gamma\gamma \to K_sK_s$ and $\pi^+\pi^-$, favors the interpretation as a non-$q\overline{q}$ [8]. It turns out that the decay of $f_0(1500)$ to $K\overline{K}$ is inconsistent with $s\overline{s}$ member of a nonet and the resonance has been considered to be the best candidate for a scalar glueball. However, one would expect the decay to $K\overline{K}$ should not be suppressed with respect to $\pi\pi$ if it is a pure glueball [1]. From the experiment, the observed branching ratios are

$$B(f_0(1500) \to \pi\pi : KK : \eta\eta : \eta\eta') = 5.1 \pm 2.0 : 0.71 \pm 0.21 :\equiv 1 : 1.3 \pm 0.5 \tag{1.6}$$

This branching fractions are not consistent with a flavour blind decay (Equation 1.3) but with a the mixing mechanism scheme (Equation 1.4).

1.3.3. The $f_0(1710)$

There is still not an agreement about the nature of the $f_0(1710)$. Different experiments gave different masses, widths and spin-parities. The latest analysis of the $J/\psi \to \gamma K\overline{K}$ by the MarkIII collaboration prefers $J^P = 0^+$ over an earlier assignment of 2^+ [8]. PWA of $J/\psi \to \gamma K\overline{K}$, $\gamma\pi\pi$, $\omega\pi^+\pi^+$, ωK^+K^-, $\phi\pi^+\pi^-$ and ϕK^+K^- decay modes were carried out by the BesII collaboration : in all decay modes, except ϕK^+K^-, the mass of $f_0(1710)$ was determined around 1700 MeV. In the ϕK^+K^- channel, a resonance in 1790 MeV was observed. In that analysis it has been claimed that $f_0(1790)$ is distinct from the $f_0(1710)$ [4].

1.4. The Physics Goals of The Present Analysis

The present work investigates the resonances formed in the decay of J/ψ to $\phi\, K_s\, K_s$ with the huge data samples of the e^+e^- collisions collected in 2009 (223.7×10^6 events) and 2012 (1.086×10^9 events) at BEPCII in Beijing [15,16]. The unprecedented statistics offers the opportunity to understand the nature of the scalar glueball and tetraquark candidates of $f_0(980)$, $f_0(1370)$, $f_0(1500)$ and $f_0(1710)$. A similar channel, $J/\psi \to \phi\, K^+\, K^-$, was analyzed by BESII Collaboration in 2005 with lower statistics [4]: a partial wave analysis of $J/\psi \to \phi\, K^+\, K^-$ and $\phi\pi^+\,\pi^-$ from a sample of 58M J/ψ events was presented. $f_0(980)$ was observed clearly in both sets of data and parameters of the Flatte formula describing the shape of the resonance were determined. A scalar state in $\pi\pi$ with $M = 1790^{+40}_{-30} MeV/c^2$ and $\Gamma = 270^{+60}_{-30}$ MeV was observed. The spin of this state is preferred 0 over 2. Its mass and width are above the average nominal values of $f_0(1710)$ therefore they claim that $f_0(1790)$ state is distinct from $f_0(1710)$. Our main aim is to improve and confirm this study with new and high statistics BESIII data. In addition we do also aim to improve the measurement of the tensor states ($J^{PC} = 2^{++}$) like $f_2(1270)$, $f_2'(1525)$ and $f_2(1810)$.

Before studying these resonances, a detailed background study, which includes an inclusive MC data sample of 1.25×10^9 events, is to be perfomed.

2. EXPERIMENT

2.1. BESIII Experiment at Institute of High Energy Physics In Beijing

The BESIII (Beijing Electron Spectrometer III) is the main detector located at the Institute of High Energy Physics In Beijing, China. The Beijing Electron Positron Collider II (BEPCII), which is an e^+e^- storage ring, is operating in the center of mass energy range 2 GeV to 4.6 GeV. The peak luminosity of BEPCII in the center of mass energy about 3.7 GeV is approximately $10^{33}\text{cm}^{-2}\text{s}^{-1}$ [17]. The experiment is designed for studying charmonium physics, D-physics, spectroscopy of light hadrons and τ-physics [8].

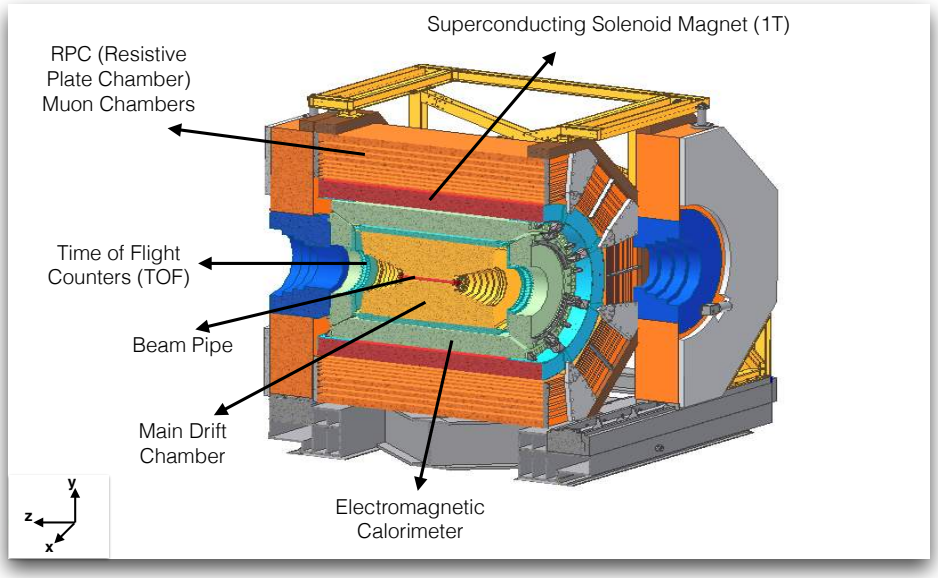

Figure 2.1. BESIII Sub-Detectors [2].

The detector consists of cylindrical multilayer drift chambers surrounded by plastic scintillators for the time-of-flight measurement of charged particles. The energy and the position of the electromagnetic showers are measured by a CsI(TI) crystal calorimeter located inside a large superconducting solenoid magnet which generates a 1T magnetic field. Muons are identified by an array of resistive plate chambers.

2.2. Main Drift Chamber

One of the most important sub-detectors for the topic of this thesis is the main drift chamber (MDC). The MDC has a small cell design with 43 sense wire layers and an almost square shape of a drift cell. Each sense wire is surrounded by 8 field wires. The average half-width of a drift cell (distance of sense wire to field wire) is approximately 6 mm in the inner chamber and about 8 mm in the outer chamber [8]. The MDC reconstructs charged tracks in 3D space. The momentum of charged particles produced at the interaction point (IP) is determined with the help of the 1.0 Tesla magnetic field that is present throughout the tracking volume. The MDC also measures energy loss, dE/dx, to identify charged particles. A single wire resolution is better than 130μm and dE/dx resolution is better than 6%. The momentum resolution is better than 0.5% for charged tracks with a momentum of 1 GeV. At such low momenta, the amount of material in the volume of the MDC must be kept to a minimum to reduce multiple Coulomb scattering effects. A helium based gas mixture He-C_3H_8 $60:40$ was chosen to minimize the effect of multiple scattering while maintaining a reasonable dE/dx resolution [17]. Polar angle coverage of the MDC is $|\cos\theta| < 0.93$ [8]. The MDC also produces signals for the level 1 triggers to select good physics events and reject various backgrounds, which are not due to J/ψ decays [17].

The start point of the MCD tracking algorithm is the formation of track segments from hits via pre-calculated patterns. Then, algorithm links the found axial segments to circular tracks and applies a circular fit using the least-square method [8]. An iterative helix fit is performed on the track candidates. As a last step, a track refitting procedure based on the Kalman-filter technique is performed after collecting additional hits that might possibly belong to the track. The algorithm can maintain a tracking

efficiency of more than 98% for $p_T > 150$ MeV/c [8].

2.2.1. The dE/dx Measurement

The energy loss in the Main Drift Chamber (MDC) provides valuable information for particle identification (PID). The normalized pulse height, which is proportional to the energy loss of incident particles in the drift chamber, is a function of $\beta\gamma = p/m$, where p and m are the momentum and mass of a charged particle [8]. Figure 2.2 shows the normalized pulse height versus momentum of different particles.

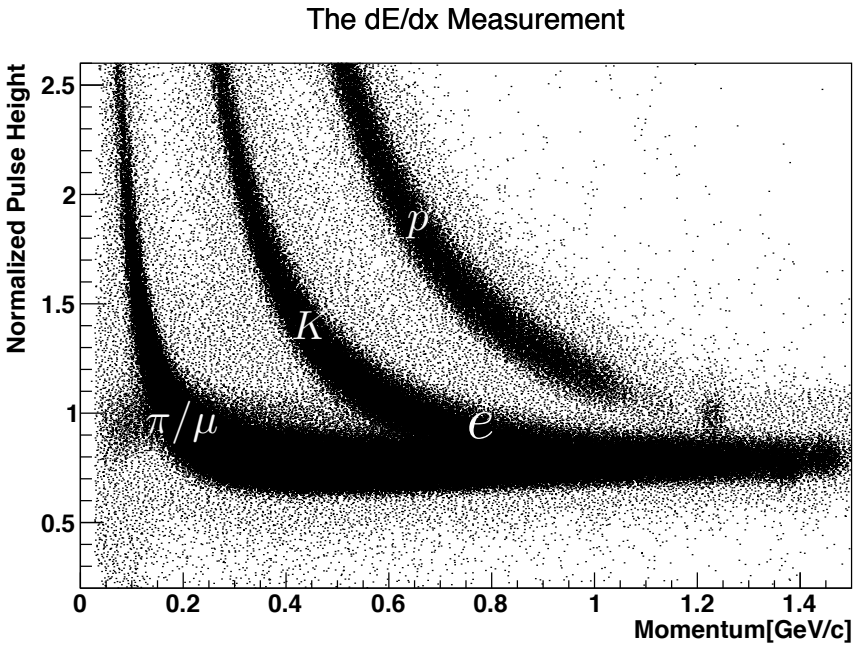

Figure 2.2. The normalized pulse heights (dE/dx) vs. momentum of charged particles.

2.2.2. Expected Momentum Resolution

With a uniform axial magnetic field used for bending the particles along with equally spaced wire layers, transverse momentum of the particles can be measured

with a resolution of :

$$\frac{\sigma_{p_t}}{p_t} = \sqrt{\left(\frac{\sigma_{p_t}^{wire}}{p_t}\right)^2 + \left(\frac{\sigma_{p_t}^{ms}}{p_t}\right)^2} \tag{2.1}$$

where p_t is the transverse momentum of particles, $\sigma_{p_t}^{wire}$ is the momentum resolution due to the uncertainties of position measurements of individual wires and $\sigma_{p_t}^{ms}$ is the momentum resolution resulting from multiple scattering of tracks inside the tracking chamber [17]. $\sigma_{p_t}^{wire}/p_t$ can be calculated as

$$\frac{\sigma_{p_t}^{wire}}{p_t} = \frac{3.3 \times 10^2 \times \sigma_x}{B \times L^2} \times p_t \times \sqrt{\frac{720}{n+5}}. \tag{2.2}$$

where σ_x is the resolution of a single wire in meters, B is the magnetic field in Tesla and L is the track length in meters, p_t is the transverse momentum of the particles in GeV/c and n is the total number of wire layers [17]. The term for multiple scattering is calculated by,

$$\frac{\sigma_{p_t}^{ms}}{p_t} = \frac{0.05}{B \times L} \times \sqrt{1.43\frac{L}{X_0}}\left(1 + 0.038 \ln \frac{L}{X_0}\right) \tag{2.3}$$

where X_0 is the radiation length in meters of the material assumed to be uniformly distributed inside the tracking volume. β ($\beta = v/c$) is assumed to be 1. Using the

Table 2.1. Values for MDC.

n	43
L (at 90°)	70 cm
p_t	1 GeV/c
B	1 Tesla
σ_x	130μm

properties of the MDC as tabulated in Table 2.1, we obtain $\sigma_{p_t}^{wire} = 0.32\%$ and $\sigma_{p_t}^{ms} = 0.35\%$. The expected momentum resolution of the MDC for a 1 GeV track at $\theta = 90°$,

where θ is the polar angle.

$$\sigma_{p_t} = \sqrt{\sigma_{p_t}^{ms} + \sigma_{p_t}^{wire}} = \sqrt{0.35\% + 0.32\%} = 0.47\% \tag{2.4}$$

Based on this calculation, the momentum resolution of the MDC is expected to be better than 0.5% at p_t=1 GeV [17].

2.3. Time of Flight System

The Time-of-Flight (TOF) detector measures the flight time of charged particles. TOF information is combined with the dE/dx measurement from the MDC to improve the particle identification (PID). It is composed of plastic scintillator bars and read out by fine-mesh phototubes [8]. TOF detector is placed between the drift chamber and the electromagnetic calorimeter. TOF System is composed of two subsystems: barrel and endcap. The solid angle coverage of the barrel TOF is $|\cos\theta| < 0.83$, while that of the endcap is $0.85 < \cos\theta < 0.95$. The total time resolution of for double layer barrel and the endcap is expected to be about 100ps [8].

The velocity (βc) and the mass (m) of the charged particle can be calculated from [8]:

$$\beta = \frac{L}{c \times t_{mea}} \tag{2.5}$$

$$m^2 = p^2 \times \frac{1 - \beta^2}{\beta^2} \tag{2.6}$$

where t_{mea} is the measured time-of-flight, L and p are the corresponding flight path length and the momentum of the charged particle provided by the MDC measurements, and c is the velocity of light in vacuum. Figure 2.3 shows the typical mass square distributions for electrons, pions, kaons and protons in different momentum ranges.

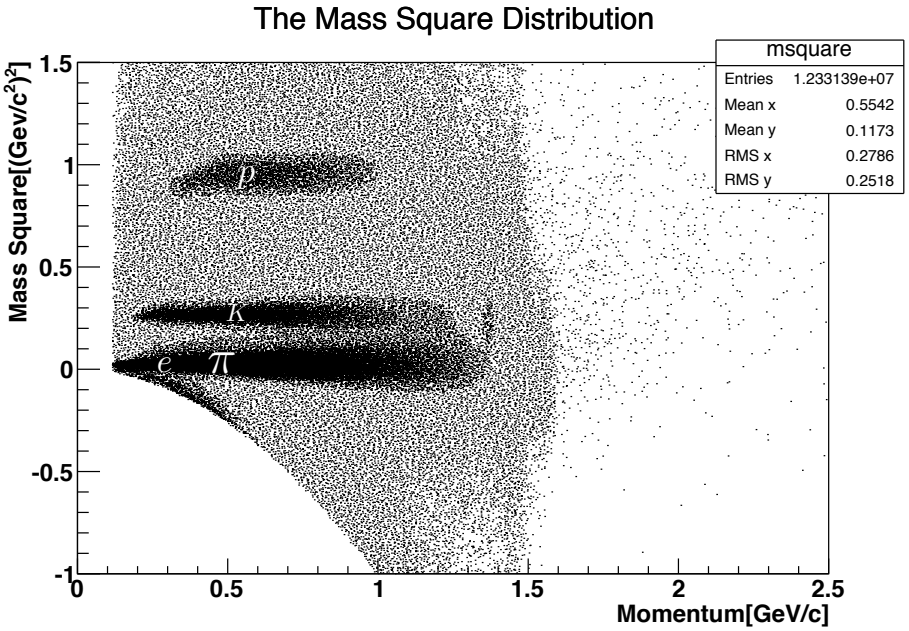

Figure 2.3. The mass square distribution from TOF measurements.

2.4. Electromagnetic Calorimeter

The main target of the electromagnetic calorimeter (EMC) is to measure precisely the energies of photons above 20 MeV and to provide trigger signals. For π/e separation, it has a good capability for momenta higher than 200 MeV [17]. The EMC consists of 6240 large CsI(TI) crystals located outside of the TOF counters and inside of the coil of the solenoid. The energy resolution of the EM showers is $\sigma_E/E = 2.5\%\sqrt{E}$ and the position resolution is $\sigma = 0.6$ cm$/\sqrt{\mathrm{E}}$, where E is in GeV [17]. The angular coverage of the EMC-barrel part is $|\cos\theta| < 0.83$. For the endcaps, the angular coverage is $0.85 < |\cos\theta| < 0.95$ [17].

2.5. Muon Identifier

The muon identifier is the outer most part of the BESIII detector. Ultimate aim for the Muon Identifier is to measure the positions and the trajectories of muons produced in e^+e^- collisions. They can be identified with low cut-off momentum via

series of resistive plate chambers (RPCs) which are inserted in the steel plates of the magnetic flux return. Muon Identifier is divided into eight segments for the barrel and four segments for the endcap. RPC superlayer modules (SM) are located in the gaps between two steel plates of each segment. They consist of double gap RPC counters. The reconstructed tracks in the MDC and the energy measured in the EMC are combined with hits in muon counters to identify muon above a cut-off momentum 400 MeV [17].

2.6. Trigger and Data Acquisition System

Since BESIII experiment is a charm-factory, it must work in a high-event-rate and high-background-rate environment with high reliability and also the detector must process a large amount of data in real time. The trigger, data aquisition and online computing systems are designed for the purpose of accommodating multi-beam bunches separeted by 8ns and high data rate [17]. All readout electronic systems are pipelined to allow a nearly dead time free operation. To achive this aim, BESIII trigger system consists of two levels of trigger systems.

The Level 1 (L1) is a hardware trigger. At L1, sub-triggers are generated by the TOF, MDC and EMC sub-detectors and are processed by the global trigger logic [17]. The next level trigger (L3) runs on an online computing farm and it is called the software trigger. The online computer farm is designed to read out large amounts of data from the front-end electronics system for event filtering and recording valid data into permanent storage devices [17].

2.7. BESIII Offline Software

The BESIII Offline Software System (BOSS) is a complete package for data processing and physics analysis. It uses the C++ language and object-oriented techniques and runs primarily on Scientific Linux at CERN (SLC) [8]. Three types of persistent event data have been defined in the BOSS system: raw data, reconstructed data and Data-Summary-Tape (DST) data. Both reconstructed data and DST data are in

ROOT [18] format for easy management and usage [8].

BOSS system consists of five functional parts: framework, simulation, reconstruction, calibration and analysis tools. The BESIII detector simulation is perfomed by the GEANT4 [19] package. For reconstruction, BOSS reconstruction package consists mainly of the following four parts: a) a track-finding algorithm and a Kalman-Filter-based track-fitting algorithm to determine the momentum of charged particles; b) a particle identification algorithm based on dE/dx and Time-Of-Flight (TOF) measurements; c) a shower finding algorithm for electromagnetic calorimeter energy and position measurements; d) a muon track finder [8]. Moreover, it contains an event timing algorithm for determining the corresponding beam bunch crossing and also there is a secondary vertex and track refitting algorithm.

2.8. Summary of BESIII Detector

Here is the summary of the performance of the BESIII detector components [17]:

Table 2.2. Detector parameters and performace.

Sub-System		Value
MDC	Single wire $\sigma_{r\phi}(\mu\text{m})$	130
	σ_p/p (at 1 GeV)	0.5 %
	$\sigma(dE/dx$ [MeV/cm])	6%
EMC	σ_E/E (at 1 GeV)	2.5 %
	Position resolution (at 1 GeV)	0.6 cm
TOF	σ_T(ps) for Barrel	100
	σ_T(ps) for Endcap	110
Muon Id	No. of layers (barrel/end cap)	9/8
	cut-off momentum (MeV)	400
Solenoid Magnet Field (T)		1.0
Angular Coverage	$\Delta\Omega/4\pi$	93%

3. ANALYSIS AND RESULTS

3.1. Data Set, Statistics and Selection

In this analysis, the BESIII offline software system (BOSS) is used [8]. The full dataset of J/ψ is located on a common location in IHEP Computer Farms allowing users to run their own analysis code for specific studies. About 5.3×10^9 e^+e^- data were collected with the BESIII detector in 2009 and 2012, which corresponds to about 1.3×10^9 J/ψ events [16]. These data samples were processed with BOSS 6.6.4 [20].

For the $J/\psi \to \phi K_s K_s$, $\phi \to K^+K^-$, $K_s \to \pi^+\pi^-$ decay modes, we require 6 charged tracks. In the $\phi K_s K_s$ final state, we distinguish the longer living $K_s \to \pi^+\pi^-$ secondary vertex from the primary vertex of the $\phi \to K^+K^-$ decay. Charge conservation imposes that the total charge of these 6 tracks is zero. Therefore, "$\sum Q = 0$, $\#goodtracks = 6$" selection criteria is imposed. "*Good track*" just signifies that successful reconstruction of a track is selected. Particle identification (PID) is needed to distinguish the 4 pions from the 2 kaons. This is achieved by combining the energy deposition measurements (dE/dx) from the Main Drift Chamber with the time of flight information from the TOF system.

Kinematic fitting is a mathematical algorithm in which one uses the physical law governing a particle interaction or decay to improve the measurements. Many constraints can be used in the kinematic fitting. For this analysis, we use first the common space constraints of the $\pi^+\pi^-$ pair from the K_s decay and the alignment of its momentum vector with the position vector. Second, we use four momentum and energy constraints (4C). When tracks are refitted with *renewed* (i.e with more precise information) parameters, mass and momentum resolution of the ϕ and K_s mesons are improved. The kinematic fit improves also the signal to background ratio and may also elevate marginal signals to statistically significant results [8]. Detailed information about the kinematic fit is presented in Section 3.2.

The reconstruction of vertices is performed by least-squares and Kalman methods. [8] The vertex reconstruction is a mathematical procedure in which one uses the geometric constraints in order to better understand particle interaction or decay. This is achieved by the VertexFit and *SecondVertexFit* packages in BOSS. In the VertexFit package, it is assumed that each input-track originated from a common vertex and the output is the common vertex with the information of renewed input parameters. Whereas in the SecondVertexFit package, the particle with the secondary vertex is handled. The input requires production point, decay point, the four-momentum at decay point and the output is decay length in flight with the information of renewed input parameters [21]. $\phi \to K^+K^-$ decay vertex is determined by the VertexFit package, while $K_s \to \pi^+\pi^-$ decays are fitted with SecondVertexFit package. Events with converging fits are accepted. For each event, one primary vertex and two secondary vertex fits are performed. For primary vertices, $V_{xy} = \sqrt{V_x^2 + V_y^2} < 1.0$ cm, $V_z < 5.0$ cm, where V_{xy}, V_z are the vertex positions in x-y and z-direction, respectively. K_s can decay outside of these limits so those selections are not applied to *secondary vertices*. Reconstructed vertex positions for K_s and ϕ decays are shown in Figure 3.1.

The 4C fit is applied to the two K_ss, K^+ and K^-, with the additional constraints that the center of mass energy of the collision is 3.097 GeV and $(P_x, P_y, P_z) = (0.034, 0.00, 0.00)$ GeV. The initial boost in the x direction is due to the non-zero crossing angle between the two beams, which is about 2mrad [8]. Only those events with a convergent 4C fit with a χ^2 less than 50 are kept. The *four vector* information of final state particles are stored in ntuple format for further analysis.

With the two charged kaons and four charged pions, there are two combinations to form $J/\psi \to \phi K_s K_s$ final state. One is $\phi(\to K^+K^-)K_{s1}(\to \pi_1^+\pi_1^-)K_{s2}(\to \pi_2^+\pi_2^-)$ and the other is $\phi(\to K^+K^-)K_{s1}(\to \pi_1^+\pi_2^-)K_{s2}(\to \pi_2^+\pi_1^-)$. The mass distribution of the K^+K^- pair is shown in Figure 3.2. The mass distribution of the first $\pi^+\pi^-$ combination is shown in Figure 3.3 (blue line). In this figure, one can see a pronounced peak at 497 MeV which is due to the $K_s \to \pi^+\pi^-$ decay. In addition, one peak and one shoulder due to $\rho^0(770)$ and $f_0(980)$ are also visable. ϕ meson is selected by requiring $|M_{K^+K^-} - 1.019| < 0.0015$ GeV (yellow shaded area in Figure 3.2) and the $\pi^+\pi^-$ mass

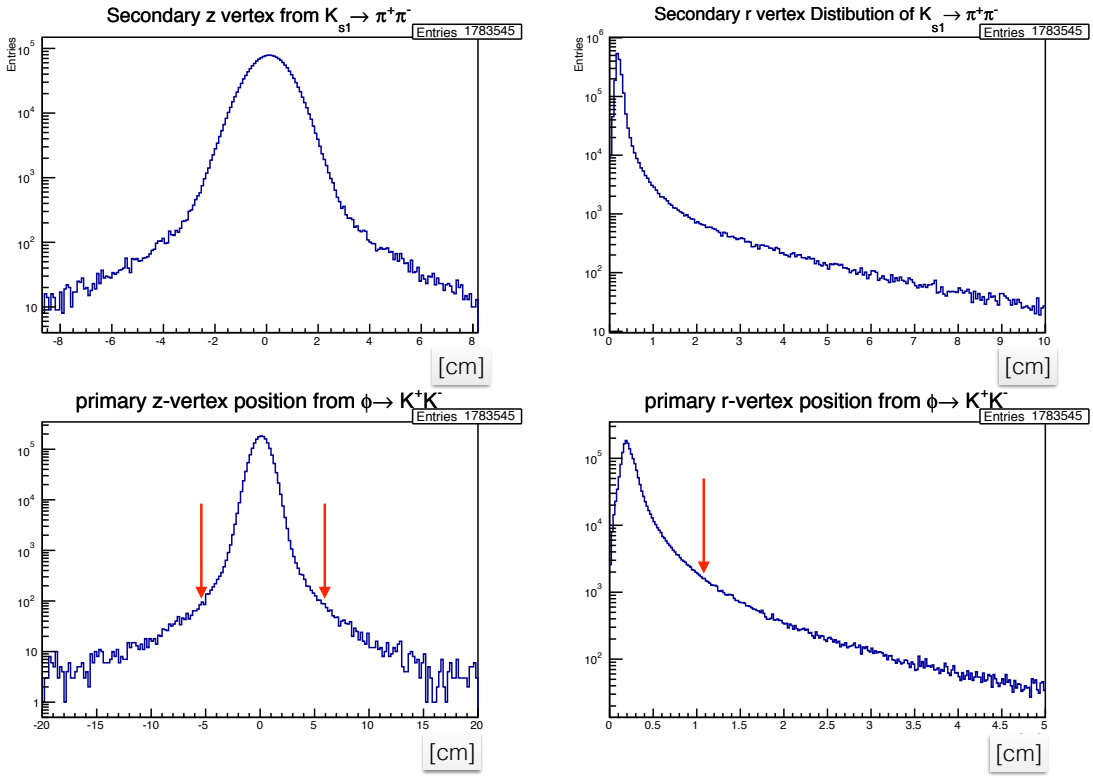

Figure 3.1. Vertex Distributions. z-vertex : z-position of the reconstructed vertex. r-vertex : transverse position (x-y plane) of the reconstructed vertex.

distribution after this ϕ mass window requirement is plotted again in Figure 3.3 (red line). A considerable amount of background is removed but some is still present. The selectiveness of the $\phi K_s K_s$ channel is visible once we redraw the $\pi_1^+\pi_1^-$ ($\pi_1^+\pi_2^-$) after the $|M_{\pi_2^+\pi_2^-}\ (\pi_2^+\pi_1^-) - 0.497| < 0.020$ GeV cut. The $M_{\pi^+\pi^-}$ invariant mass shows an almost background free peak at K_{s1} (black line).

A $\chi^2 < 50$ (of the kinematic fit) cut was applied, optimizing the signal relative to the background in an inclusive MC study (see Section 3.6.1). The number of events having the K^+K^- mass in the mass ϕ mass range is 162055. Among those, 14952 events have at least one of the two $\pi^+\pi^-$ mass combinations in the two K_ss mass windows. Only 19 events have both of the two $\pi^+\pi^-$ mass combinations within the K_ss mass windows. Since this is only a very small fraction of the total number of events selected, these events are rejected from the final sample. After applying all the mentioned selections, 14933 events remain in the $\phi K_s K_s$ channel. Full statistics are given in Table 3.1.

Table 3.1. Selection Criteria Applied on Real Data.

# processed events	5.35×10^9
$\sum Q = 0$, $\#good\,tracks = 6$	1.22×10^8
$PID:\ K^+, K^-,\ 2\pi^+,\ 2\pi^-$	6.43×10^6
one primary(ϕ) and two secondary (K_s,K_s) successful vertex fits	6.20×10^6
$4C\ Fit$	1782919
primary vertex position, $z < 5$ cm	1781785
primary vertex position, $r < 1$ cm	1717890
$\chi^2 < 50$	1315895
$\lvert M_{K^+K^-} - 1.020\rvert < 0.015$ GeV	162055
$\lvert M_{\pi_i^+\pi_j^-} - 0.497\rvert < 0.020$ GeV, one or two combinations	14952
$\lvert M_{\pi_i^+\pi_j^-} - 0.497\rvert < 0.020$ GeV, two combinations	19
$\lvert M_{\pi_i^+\pi_j^-} - 0.497\rvert < 0.020$ GeV, one combination only	14933

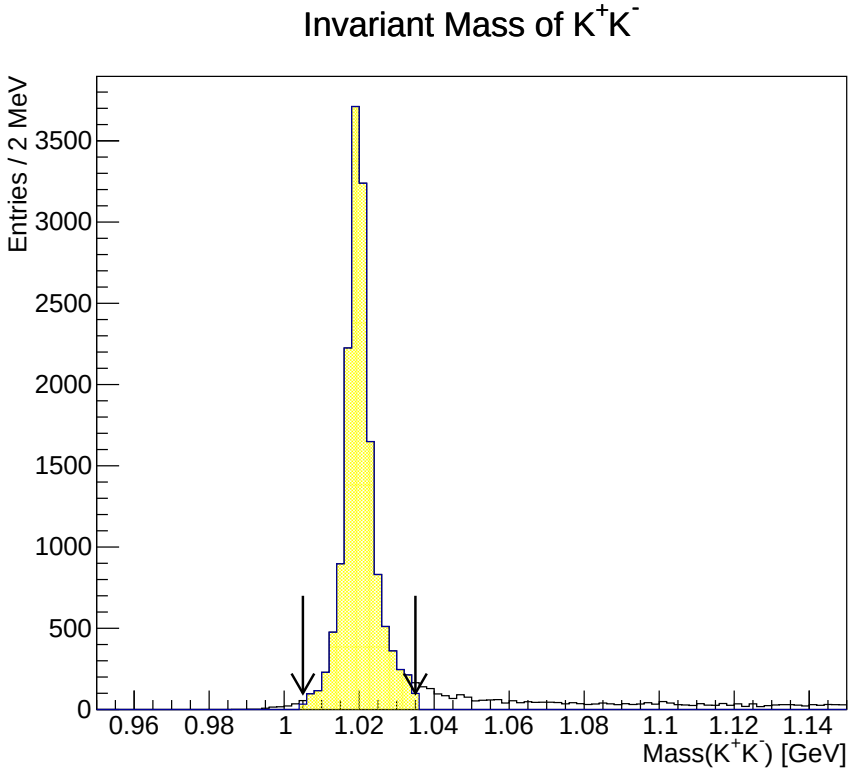

Figure 3.2. Invariant mass of K^+K^-. ϕ meson is selected by requiring a window mass cut of $|M_{K^+K^-} - 1.020| < 0.015$ GeV.

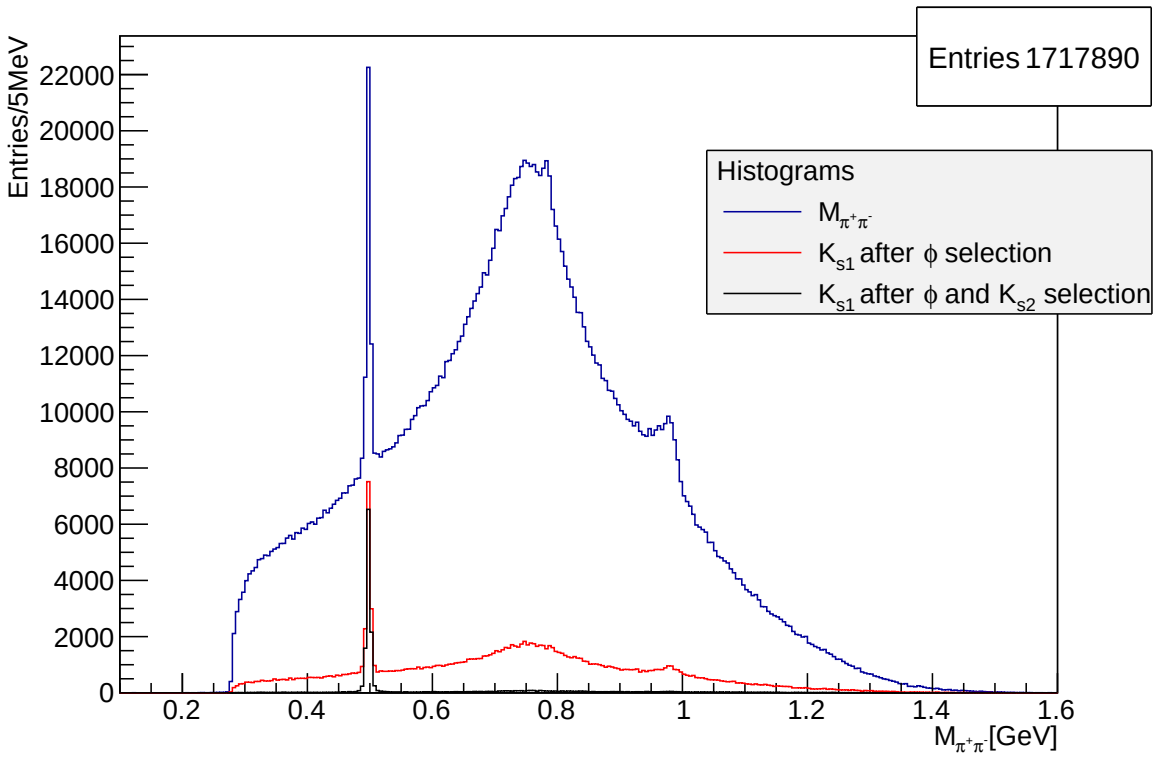

Figure 3.3. Invariant mass of $\pi^+\pi^-$ before (blue line), after ϕ meson mass cut(red line) of $|M_{K^+K^-} - 1.020| < 0.015$ GeV, and after K_s meson mass cut (black line) on the second $\pi^+\pi^-$ mass pair.

3.2. Kinematic Fit

3.2.1. General Algorithm

Kinematic fitting is used in many physics analysis in the BESIII experiment. Information gathered by Main Drift Chamber (MDC) and Electromagnetic Calorimeter (EMC) is employed by kinematic fitting. Fundamental physics laws are utilized to constraint the decay process and then improved particle parameters are obtained. We describe here more in detail the algorithm used for the helix track fit and four momentum fit after energy and momenta constraints.

To deal with various types of constraints, the Lagrange multiplier method is performed. The final equations which is used in the kinematic fitting can be written as [22]:

$$\alpha = \alpha_0 - V_{\alpha_0} D^T \lambda, \tag{3.1}$$

$$\lambda = V_D(D\delta\alpha_0 + d), \tag{3.2}$$

$$V_\alpha = V_{\alpha_0} - V_{\alpha_0} D^T V_D D V_{\alpha_0} \tag{3.3}$$

where α represents the particle parameters after the kinematic fit, α_0 means initial particle parameters before the kinematic fit, α_A is the expanding point to the constraint equations, $\delta\alpha_0$ is the difference between α and α_A, V_{α_0} is the error matrix of initial particle parameters, V_α is the updated error matrix, λ is Lagrange multiplier and $V_D = (DV_{\alpha_0}D^T)^{-1}$ is the $m \times m$ constraint covariance matrix. D and d are used to linearize the constraint equations. The χ^2 is calculated as [22],

$$\chi^2 = \lambda^T V_D^{-1} \lambda = \lambda^T (D\delta\alpha_0 + d) \tag{3.4}$$

3.2.2. Track Parameter Representation

For a track representation, the four-vector format is utilised in the BESIII experiment. It is defined as $\alpha = (p_x, p_y, p_z, E)$ in the BESIII kinematic fitting software package. A charged track is represented with 5-helix parameters in the MDC track fitting program. The relation of helix and 4-momentum [22],

$$\alpha_0 = \begin{pmatrix} p_{0_x} \\ p_{0_y} \\ p_{0_z} \\ E_0 \end{pmatrix} = \begin{pmatrix} -\sin\phi_0 \cdot Q/\kappa \\ \cos\phi_0 \cdot Q/\kappa \\ \lambda \cdot Q/\kappa \\ \sqrt{(1+\lambda^2)/\kappa^2 + m^2} \end{pmatrix} \tag{3.5}$$

where ϕ_0 is the track direction polar angle, κ is the radius of helix, λ is the track direction closest to the z-axis point, Q is the charge of the particle and m is the mass of the particle. The 4-momentum covariance matrix is obtained from,

$$V_W = J_W \cdot V_{helix} \cdot J_W^T \tag{3.6}$$

where J_W is the Jacobian matrix.

3.2.3. Four Momentum Constraints (4C)

This is the most common analysis tool for most of the physics analyses at BESIII [22]. The constraints are

$$d = \begin{pmatrix} p_x - p_{cx} \\ p_y - p_{cy} \\ p_z - p_{cz} \\ E - E_c \end{pmatrix} = 0 \tag{3.7}$$

where p_{cx}, p_{cy},p_{cz} and are the momentum and energy constraints. E_c is the energy constraint.

In many analysis of J/ψ physics, 4-momentum constraints are widely used. The decay daughters are required to satisfy energy-momentum conservation. Therefore, improved momentum, enegy and mass resolutions are obtained. In addition, the 4C kinematic fit presses background contaminations of different final state particles where, for example, one pion (kaon) is misidentified as kaon (pion).

3.3. Dalitz Plot and Projections After 4C Fit

The Dalitz Plot is a visual representation of the phase space of a three-body decay. Suppose there is a *mother* particle M and it decays into three *daughter* particles labeled as 1,2,3. An intermediate resonance R can be shown as:

$$M \to 1 + R, \qquad R \to 2 + 3. \tag{3.8}$$

Basic kinematic equation of Dalitz Plot [1] is,

$$m_{12}^2 + m_{13}^2 + m_{23}^2 = W^2 + m_1^2 + m_2^2 + m_3^2 = C \tag{3.9}$$

Where $m_{ij}^2 = (E_i + E_j)^2 - (\vec{p_i} + \vec{p_j})^2$, and W is the center of mass energy of the collision. C is a constant. If invariant mass m_{12}^2 is plotted against invariant mass m_{13}^2 with $m_2 = m_3$, the Dalitz plot has a symmetric form. Any resonance originating from particles 2 and 3 show up as a diagonal band in the symmetric Dalitz plot with the equation

$$m_{12}^2 = (C - m_{23}^2) - m_{13}^2. \tag{3.10}$$

For this study, particles 1,2 and 3 are ϕ, K_{s1} and K_{s2} respectively. Center of mass energy W is 3.097 GeV. Diagonal resonances and the *symmetric* Dalitz plot is shown in Figure 3.4. As it is seen from the Dalitz plot, the most evident diagonal band is the resonance $f_2(1525)$. Apart from $f_0(980)$, which is also clearly seen in the plot, other resonances may be present. Their presence also may be inferred by examining at the

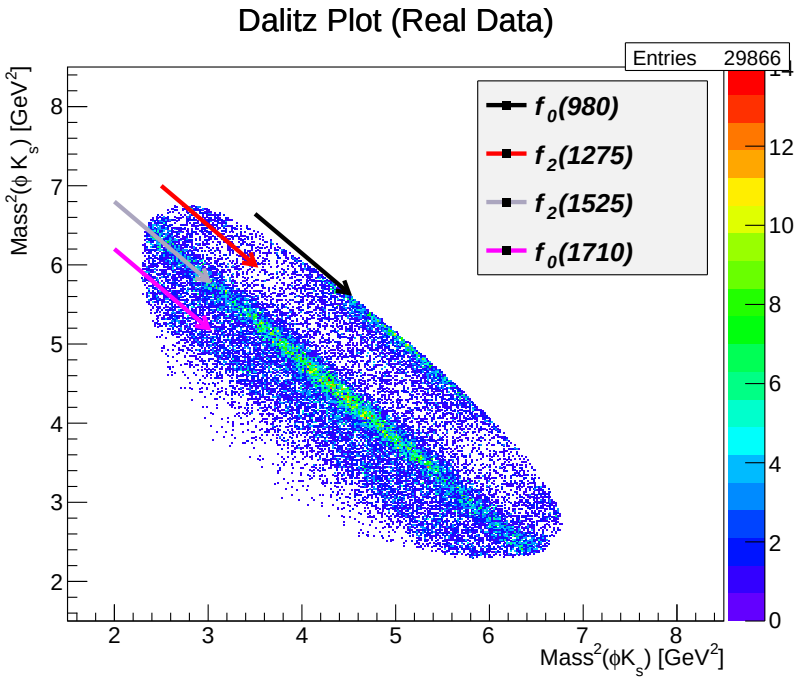

Figure 3.4. Dalitz Plot for $J/\psi \to \phi K_s\, K_s$ (Real Data). $M^2_{\phi K_{s1}}$ and $M^2_{\phi K_{s2}}$ are plotted twice on both scales (two-fold). The colors represent the nominal masses of the resonances [3].

invariant mass of K_sK_s (Figure 3.5). Projection of the Dalitz plot, invariant mass of ϕK_s, is seen in Figure 3.6. In this exotic invariant mass, we do not expect to observe any resonant states.

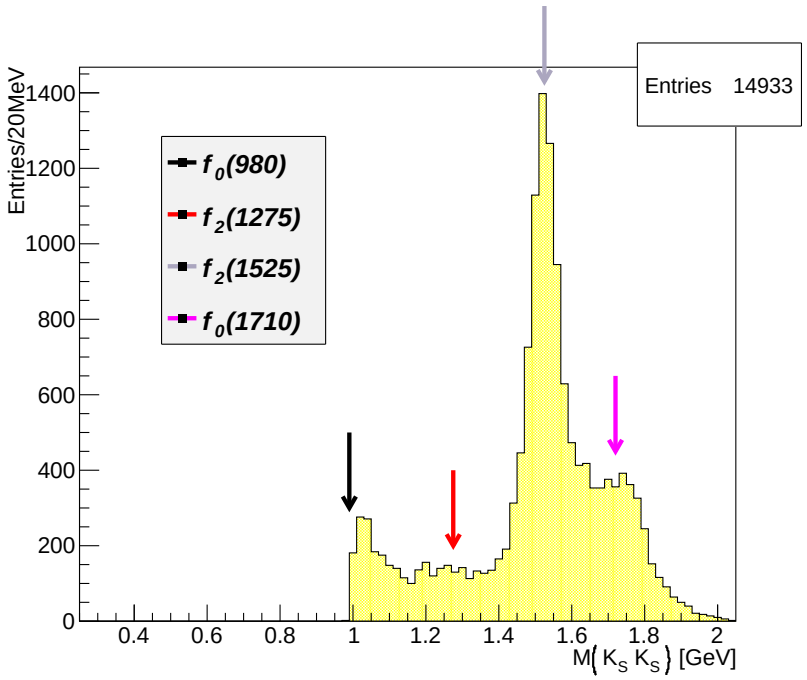

Figure 3.5. Invariant mass of $K_s\,K_s$. The colors represent the nominal masses of the resonances [3].

The Dalitz plot and the invariant mass distributions look similar to those obtained in the analysis of $J/\psi \to \phi K^+\,K^-$ performed by the BESII Collaboration [4] (See Figure 3.7). Therefore, since we have higher statistics, it is highly feasible that this channel can be used to confirm and improve their results after a Partial Wave Analysis (PWA) to be studied in a future work.

3.4. Exclusive Monte Carlo (MC) for $J/\psi \to \phi K_s\,K_s$

As they will be used as an input to PWA, exclusive MC simulation of $J/\psi \to \phi K_s\,K_s$ events were generated with BOSS version 6.6.4. The same selections as in the real data were applied to the MC events (see Table 3.2). The invariant masses, Dalitz

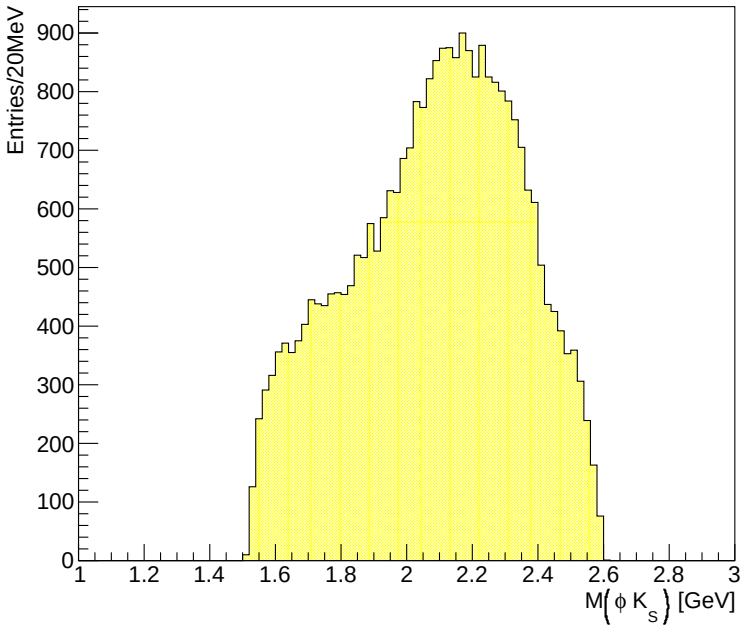

Figure 3.6. Invariant mass of $\phi\, K_s$. It is the projection of the Dalitz Plot (Figure 3.4). No intermediate resonances appear.

Table 3.2. Selection Criteria For Exclusive MC Events.

# processed events	1.47×10^7
$\sum Q = 0$, $\#good\,tracks = 6$	6.39×10^6
$PID:\ K^+, K^-,\ 2\pi^+,\ 2\pi^-$	3.58×10^6
one primary(ϕ) and two secondary (K_s,K_s) successful fits	2.90×10^6
$4C\ Fit$	2.28×10^6
primary vertex position, $z < 5$cm	2.14×10^6
primary vertex position, $r < 1$cm	2.13×10^6
$\chi^2 < 50$	2.03×10^6
$0 < \lvert M_{K^+K^-} - 1.020\rvert < 0.015$ GeV	1.90×10^6
$0 < \lvert M_{\pi^+\pi^-} - 0.497\rvert < 0.020$ GeV	1.22×10^6

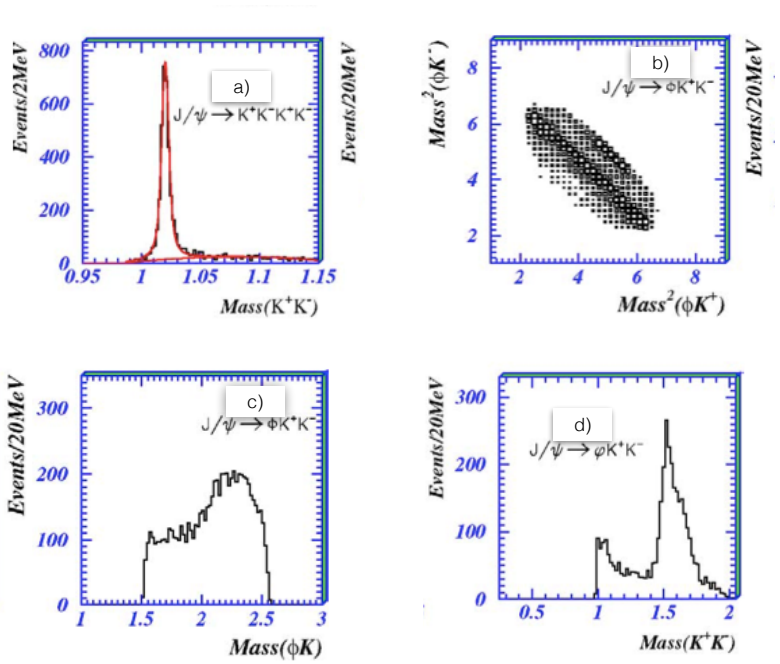

Figure 3.7. BESII Analysis of $J/\psi \to \phi K^+ K^-$: $M_{K^+K^-}$ (a), Dalitz Plot (b), $M_{\phi K^\pm}$ (c), $M_{K^+K^-}$ (d) [4].

Plot and its projection, are also plotted for exclusive MC events (Figure 3.8). The exclusive MC events are produced according to the available phase space allowed by energy and momentum conservation. They are used to evaluate the acceptance of the detector.

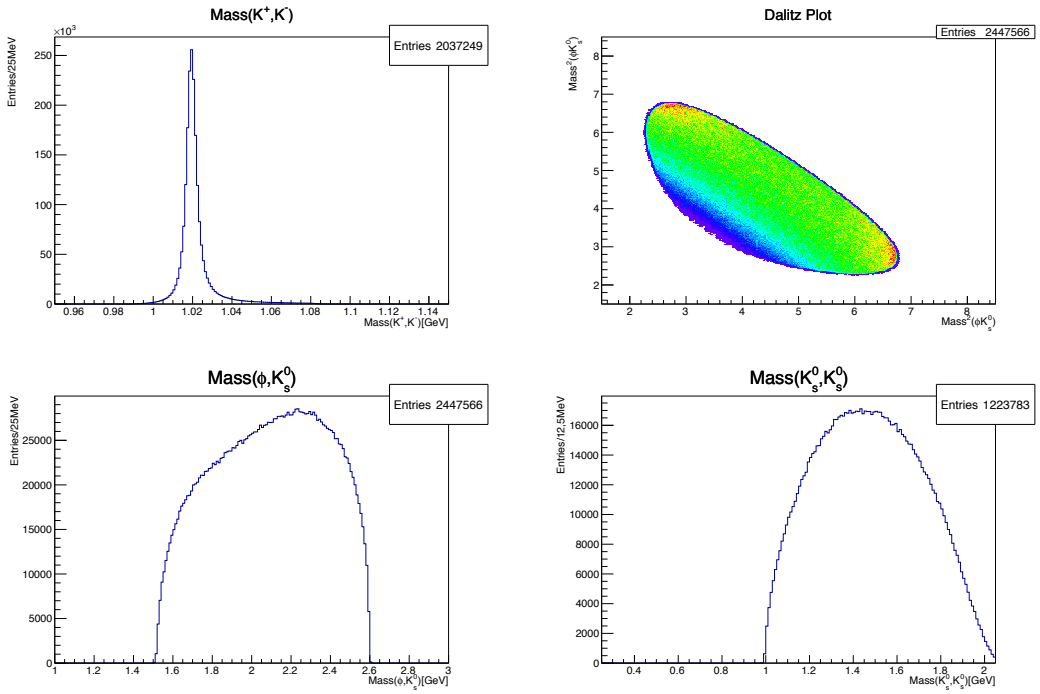

Figure 3.8. Exclusive MC: K^+K^- and, Dalitz Plot, ϕK_s and K_sK_s invariant mass. The Dalitz Plot shows a uniform distribution up to $M_{K_sK_s} \sim 1.8$ GeV.

3.5. Background Study

In this section two independent background estimates will be described. For the first estimate, an inclusive MC simulation is used while in the second estimate the contamination from other channels will be evaluated directly from the data.

3.5.1. Inclusive Monte Carlo

The default MC generator uses KKMC [23] + BesEvtGen to generate charmonium decays. The KKMC simulates the production of $c\bar{c}$ via e^+e^- annihilation including initial state radiation, while the subsequent charmonium decays are generated with BesEvtGen.

As its name suggests, inclusive MC contains all the possible decay channels of J/ψ based on decay channels listed by the Particle Data Group [24]. Inclusive MC events are constructed by the BESIII event generator (BesEvtGen) as it is described in [25] and based on EvtGen [26]. The main purpose of using inclusive MC is to estimate the contamination of other channels. To be consistent with the number of J/ψ events collected in 2009 and 2012, two samples of 225 million and 1 billion of inclusive MC events of 2009 and 2012 data, respectively, have been generated and processed with BOSS 6.6.4. To select $J/\psi \to \phi K_s\, K_s$, we perform the same cuts as in the real data. The feeddown of the background channels is categorized using the MC truth information.

In order to reduce the background and improve the quality of the data, a cut on the χ^2 is performed. Figure 3.9 shows the χ^2 distribution after 4C kinematic fit for the signal and background. Light red color represents signal channels $\phi(K_0 \to K_s)(\overline{K_0} \to K_s)$, $\phi f_2(1525)$, $\phi f_0(980)$, $\phi f_0(1500)$, $\phi f_0(1370)$, $\phi f_2(1275)$. Other colors shows the main background channels : $\phi 2\pi^+ 2\pi^-$ (black), $K^+K^- 2\pi^+ 2\pi^-$(violet), $K^{*+}\, K^{*-}\rho$(magenta), $K^+K^- f_2(1525)$(green), $f_0(1370)K\overline{K}$(light yellow), $a_0(980)K\overline{K}$(cyan), and $a_2^- K\overline{K}$, $a_2^- \to K^-K^0$ (yellow).

A $\chi^2 < 50$ cut has been perfromed. It has been shown that this value optimises the merit factor. After the χ^2 selection, the number of signal and background events are listed in Table 3.3 and 3.4, respectively. Based on these statistics, the background contribution is only 3.2%.

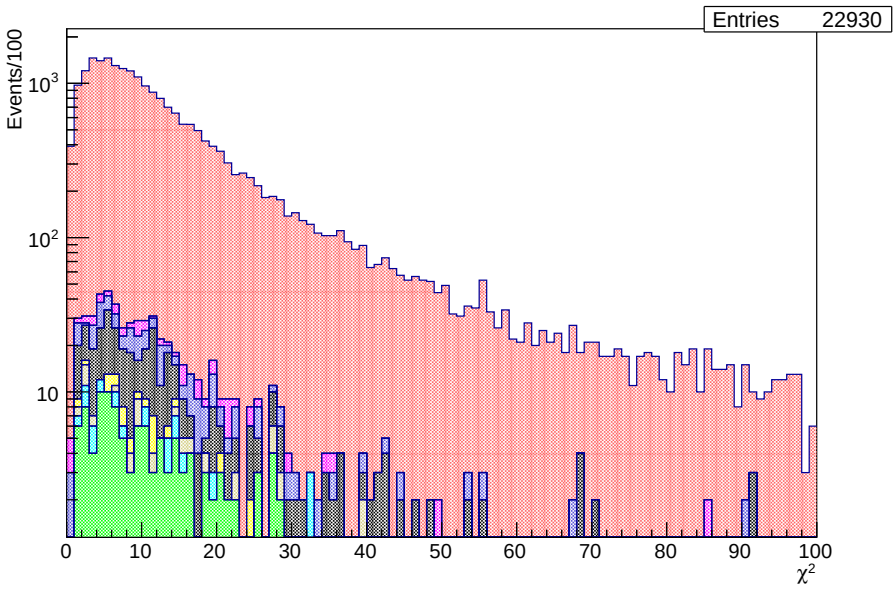

Figure 3.9. χ^2 Distribution after 4C kinematic fit of $J/\psi \to \phi K_s K_s$ in inclusive MC events. On the stacked histogram, the constribution of the signal channel $J/\psi \to \phi K_s K_s$ is shown in light red color, background channels are in black, violet, magenta, green, light yellow, cyan and yellow colors.

Table 3.3. Number of signal channels in inclusive Monte Carlo Simulation, out of 1.25×10^9 generated events.

$\phi(K_0 \to K_s)(\overline{K_0} \to K_s)$	7970
$\phi\, f_2(1525)$	6986
$\phi f_0(1710)$	4310
$\phi\, f_0(1500)$	909
$\phi\, f_0(980)$	865
$\phi\, f_0(1370)$	265
$\phi\, f_2(1275)$	205
Total	22930

Table 3.4. Number of background channels in inclusive Monte Carlo Simulation, out of 1.25×10^9 generated events.

$\phi\, 2\pi^+\, 2\pi^-$	230
$K^+\, K^-\, 2\pi^+\, 2\pi^-$	128
$K^+\, K^-\, f_2(1525)$	118
$K^{*+}\, K^{*-} \rho$	70
$K^+\, K^-\, K^0\, \overline{K^0}$	28
$a_2^+\, K^0\, K^-$, $a_2^+ \to K^+ \overline{K^0}$	25
$f_0(1370)\, K^0\, \overline{K^0}$	22
$a_0(980)\, K^0\, \overline{K^0}$	22
$a_2^-\, \overline{K^0}\, K^+,\ a_2^- \to K^-\, K^0$	20
$\phi\, f_1$, $f_1 \to \rho\pi^+\, \pi^-$	21
$K^+\, K^-\, f_0(1710)$	8
$K^{*+}\, K^{*-} \pi^+ \pi^-$	7
$\phi(K_0 \to K_l)(\overline{K_0} \to K_s)$	1
$K^+\, K^-\, f_2(1275)$	3
$\phi(K_0 \to K_s)(\overline{K_0} \to K_l)$	2
$a_0^+(980)\, K^-\, K^0$	3
$a_0^-(980)\, K + \overline{K^0}$	2
$K_1^+ \pi^- \overline{K^*}$	2
$K_1^+ \pi^- \overline{K_0(1430)}$	2
$K^+\, K^-\, f_0(1370)$	1
$b_1^-\, \overline{K^*}\, K^+$	1
$K_1'^+\, K_1'^-$	1
$K_1^-\, \rho\, K^+$	1
$K_1'^+\, K_2^{*-}$	1
$K^-\, \pi^+\, \rho\, K_0(1430)$	1
$K^-\, \rho\, K_2(1430)^+$	1
Total	790

3.5.2. Background Estimate from the Side Bins

In order to understand the background contribution of other channels' spectrum, one can select events which fall into mass intervals near the ϕ and K_s signal mass windows. These neighbouring mass windows are called sidebands. For this study, ϕ and K_s sidebands are selected as follows:

- ϕ : 1.050 GeV $< M_{K^+K^-} <$ 1.080 GeV.
- K_s : 0.547 GeV $< M_{\pi^+\pi^-} <$ 0.567 GeV.
- K_s : 0.427 GeV $< M_{\pi^+\pi^-} <$ 0.447 GeV.

After determining sideband ranges, one can compare the $M_{K^+K^-\,K_s}$ and $M_{K_sK_s}$ distributions as obtained from the sidebins, with the distributions obtained from the signal region (Figure 3.10). Likewise, we also obtain the Dalitz plot for the sidebin events. One can notice that sidebin background is almost uniformly distributed over the $M_{\phi K_s}$ invariant mass (Figure 3.10c. However, in the $M_{K_sK_s}$ mass distribution, an enchancement around 1.5 GeV is visible. This is presumably due to the decay $J/\psi \to K^+K^-f_2'(1525)$. The diagonal band $f_2'(1525) \to K_sK_s$ is also visible in the Dalitz plot from the ϕ sidebin.

In order to estimate the ϕ background from the K^+K^- invariant mass distribution, K^+K^- invariant mass distribution is fitted with a Voigtian, that is a Breit Wigner convoluted with the Gaussian, plus a Chebychev polynomial. To estimate the background, the integration of the polynomial is performed in the signal region. To take into account the phase space limitation of $\phi \to K^+K^-$, 1 million $J/\psi \to K^+K^-K_sK_s$ phase space MC events have been generated and reconstructed. The acceptance corrected K^+K^- invariant mass distribution and the fit is shown in Figure 3.11. Integration in the signal range (1.005 GeV $< M_{K^+K^-} <$ 1.035 GeV) gives a contribution of background events of about 1.2%.

The distribution of $M_{\pi^+\pi^-}$ from K_s sideband events are shown in Figure 3.12. The mass distribution is almost uniformly distributed over all of the phase space.

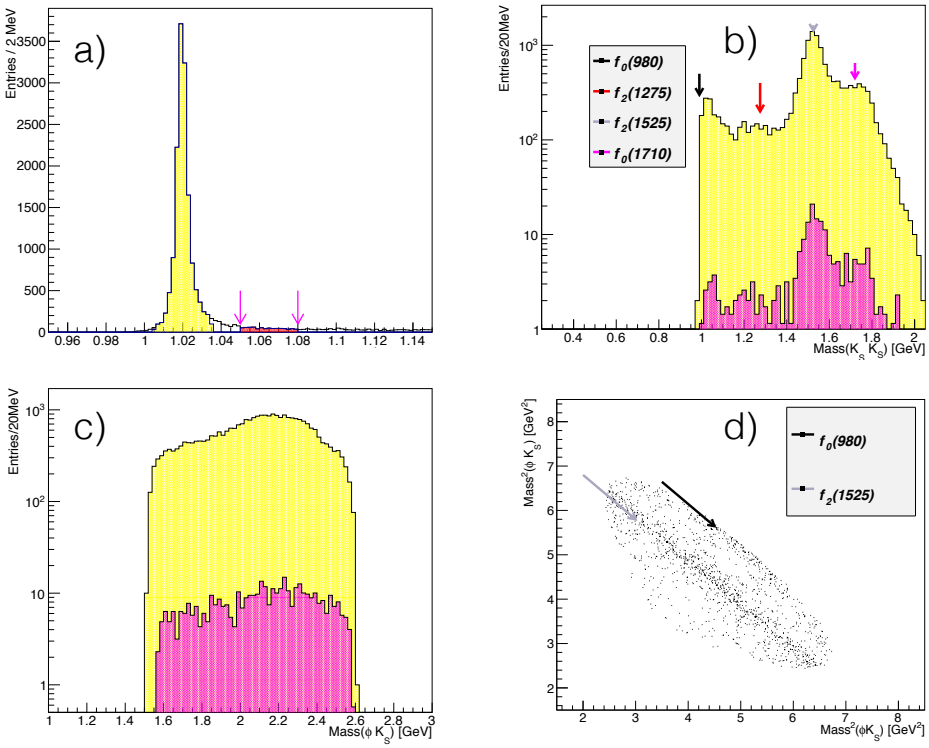

Figure 3.10. (a) $M_{K^+K^-}$ sideband events (red), (b) $M_{K_sK_s}$ with the $M_{K^+K^-}$ sideband events selected (red), arrows represent the rough locations of the peaks we identify, (c) $M_{\phi K_s}$ with the $M_{K^+K^-}$ sideband events selected (red), (d) Dalitz plot with the $M_{K^+K^-}$ sideband events selected.

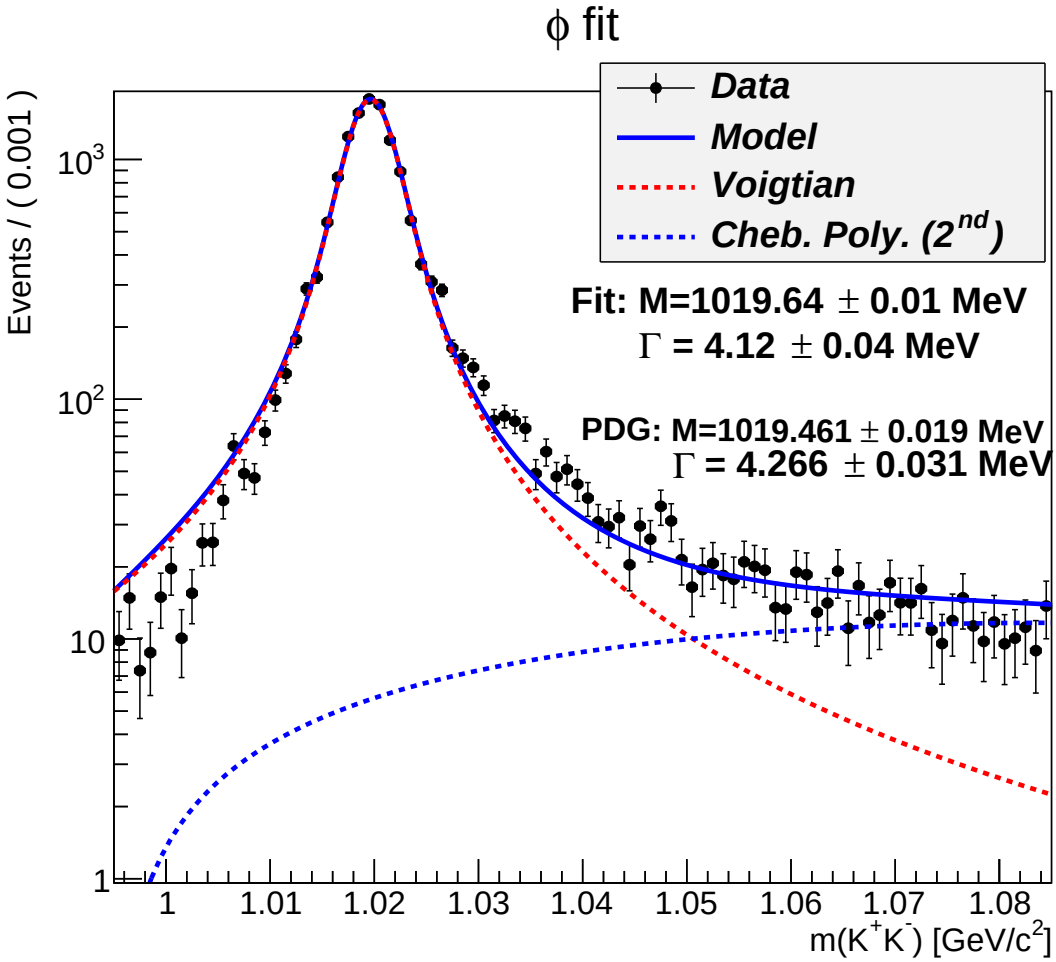

Figure 3.11. Fit of $M_{K^+K^-}$ histogram with a Voigtian function + a Chebychev polynomial (for background). The optimum in the ϕ mass is extracted as 1019.7 ± 0.5 MeV and it is in agreement with the PDG value [3].

The $M_{\pi^+\pi^-}$ invariant mass distribution has been fitted with two Gaussian functions and Chebychev polinomial. The integration in the signal mass range (0.487 GeV $< M_{\pi^+\pi^-} <$ 0.507 GeV) gives a contribution of about 1.6%.

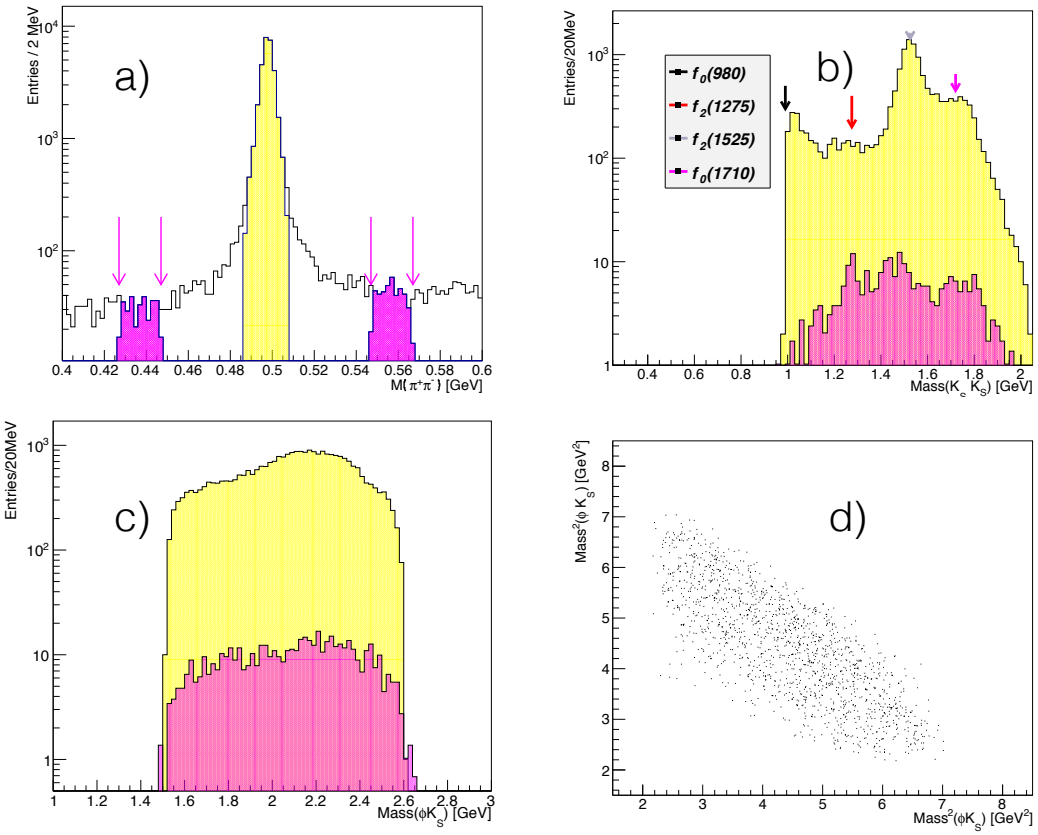

Figure 3.12. (a) $M_{\pi^+\pi^-}$ sideband events (red), (b) $M_{K_sK_s}$ with the $M_{\pi^+\pi^-}$ sideband events selected (red), (c) $M_{\phi K_s}$ with the $M_{\pi^+\pi^-}$ sideband events selected (red), d) Dalitz plot with the $M_{\pi^+\pi^-}$ sideband events selected.

Table 3.5 shows the background estimates from real data and inclusive MC. The total background contribution assuming the background from the two different fits to data are mostly orthonormal to each other is 2.8%. This is broadly consistent with estimates from inclusive MC's, which is 3.2%.

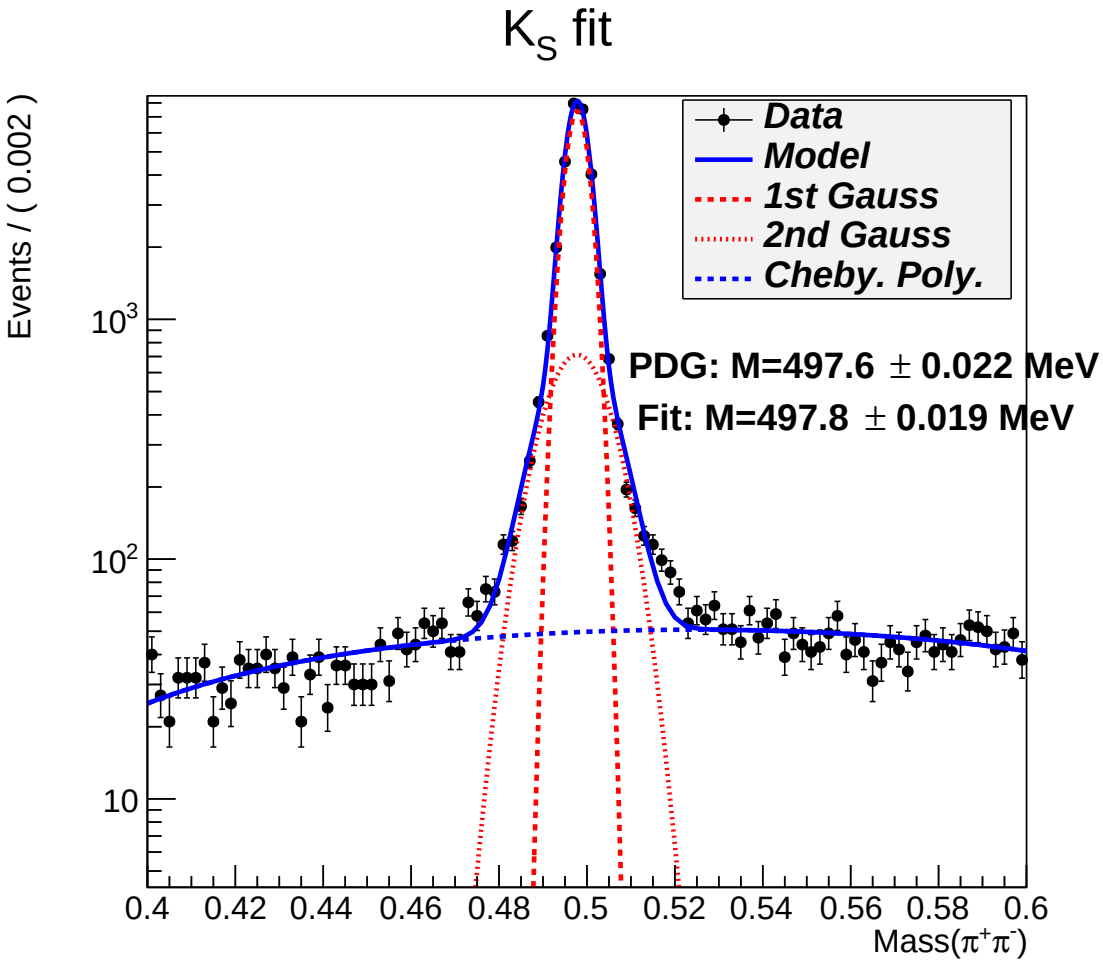

Figure 3.13. Fit of $M_{\pi_i^+\pi_j^-}$ with double Gaussian + a Chebychev Polynomial (for background). The optimum in the K_s mass is extracted as 497.8 ± 0.019 MeV and it is in agreement with the PDG value [3].

Table 3.5. Background Estimates.

Inclusive Monte Carlo	3.2%
$M_{K^+K^-}$	1.2%
$M_{\pi_i^+\pi_j^-}$	1.6%

4. CONCLUSION

Searching for undiscovered particles and performing precision measurements on light-quark sector require unambiguous determination of the properties of the ordinary mesons. This allows us to distinguish them from the glueball and tetra-quark candidates like $f_0(980)$, $f_0(1500)$, $f_0(1710)$ and others. In the decay channel of $J/\psi \to \phi K_s K_s$, the $K_s K_s$ invariant mass distribution shows similar structures to those observed in the K^+K^- mass distribution as in the study of $J/\psi \to \phi K^+K^-$ by the BESII collaboration. Since this decay channel has a displaced vertex, our results demonstrate a lower background compared to $J/\psi \to \phi K^+K^-$. Futhermore, the BESIII experiment has much more J/ψ statistics than older BESII experiment. Two independent background studies, one from inclusive MC simulation and another one from real data analysis, are consistent and gives a background level of around 3%. These estimates will be used as an input to partial wave analysis of $J/\psi \to \phi K_s K_s$.

In this preliminary work, we can already observe by eye one peak around 1 GeV and another one around 1.5 GeV, which correspond presumably to the tetra-quark candidate $f_0(980)$, $f_2(1525)$ and/or glueball candiate $f_0(1500)$. Another shoulder at 1.7 GeV is hypothesized to be $f_0(1710)$.

APPENDIX A: FORMULAS USED TO MODEL THE RESONANCE

A.1. Relativistic Breit Wigner Formula

$$f = \frac{1}{M^2 - s - iM\Gamma_{const}} \tag{A.1}$$

where s is the center-of-mass energy that the resonance is produced. M is the mass of the resonance and Γ_{const} is the resonance width.

A.2. Flatte Formula

$$f = \frac{1}{M^2 - s - i(g_1\rho_{\pi\pi} + g_2\rho_{K\overline{K}})}. \tag{A.2}$$

where ρ is a Lorentz invariant phase space $2k/\sqrt{s}$. And k refers to the π or K momentum in the rest frame of the resonance. g_1 and g_2 are coupling constants. M is the mass of resonance that will be fitted.

REFERENCES

1. Uman, I., *Antiproton-proton Annihilation in Flight Into K+K-Pi0*, Ph.D. Thesis, Ludwig Maximilian University of Munich, 2001.

2. Institute of High Energy Physics, C. A. o. S., *Brief Introduction of IHEP*, 2004, `http://www.ihep.ac.cn/english/ihep.htm`, March 2015.

3. Group, P. D., *Review of Particle Physics*, 2014, `http://pdg.lbl.gov/index.html`, March 2015.

4. Ablikim *et al.*, "Resonances in J/$\psi\rightarrow$ $\phi\pi+$ π- and ϕK+ K-", *Physics Letters B*, Vol. 607, No. 3, pp. 243–253, 2005.

5. Han, M. Y. and Y. Nambu, "Three-Triplet Model with Double SU(3) Symmetry", *Physical Review*, Vol. 139, pp. B1006–B1010, 1965.

6. Greenberg, O. W., "Spin and Unitary-Spin Independence in a Paraquark Model of Baryons and Mesons", *Physical Review Letters*, Vol. 13, pp. 598–602, 1964.

7. Ochs, W., "The Status of Glueballs", *Journal of Physics*, Vol. G40, p. 043001, 2013.

8. Asner *et al.*, "Physics at BES-III", *International Journal of Modern Physics*, Vol. A24, pp. S1–794, 2009.

9. Forkel, H., "QCD Glueball Sum Rules Revisited", *Brazilian Journal of Physics*, Vol. 34, pp. 229 – 232, 2004.

10. Toki, W., "Search for Glueballs", *Proceedings of 24th SLAC Summer Institute on Particle Physics (SSI 96), Standord, California*, 1996.

11. Close, F. E. and A. Kirk, "Scalar Glueball q Anti-q Mixing Above 1-GeV And

Implications For Lattice QCD", *European Physical Journal*, Vol. C21, pp. 531–543, 2001.

12. Abele *et al.*, "[Crystal Barrel Collaboration]", *Physical Review B*, Vol. 385, p. 425, 1996.

13. Barberis *et al.*, "[WA102 Collaboration]", *Physical Review B*, Vol. 479, p. 59, 2000.

14. Abele *et al.*, "[Crystal Barrel Collaboration]", *Physical Review B*, Vol. 380, p. 453, 1996.

15. Collaboration, B., *Beijing Electron Spectroscopy III*, 2010, `http://bes3.ihep.ac.cn`, December 2014.

16. Ablikim *et al.*, "Determination of the number of J/ψ events with J/$\psi\rightarrow$ *inclusive* decays* (Draft Paper)", *Chinese Physics C*, Vol. 33, p. Xxx, 2015.

17. Ablikim *et al.*, "Design and construction of the BESIII detector", *Nuclear Instruments and Methods in Physics Research A*, Vol. 614, pp. 345–399, Mar. 2010.

18. CERN, *ROOT*, 1995, `https://root.cern.ch/drupal/`, March 2015.

19. Agostinelli *et al.*, "Geant4—a simulation toolkit", *Nuclear Instruments and Methods in Physics Research Section A: Accelerators, Spectrometers, Detectors and Associated Equipment*, Vol. 506, No. 3, pp. 250 – 303, 2003.

20. IHEP, *BESIII Offline Software Group*, 2010, `http://docbes3.ihep.ac.cn/ offlinesoftware/index.php`, August 2014.

21. IHEP, *BESIII Offline Software Group, Vertex Fit Package*, 2010, `http://docbes3.ihep.ac.cn/ offlinesoftware/index.php`, August 2014.

22. Liang, Y., H. Rang-Lin, L. Wei-Guo, B. Jian-Ming, F. Cheng-Dong, H. Bin, L. Ying, L. Qi-Wen, N. Fei-Peng, S. Sheng-Sen, X. Min, Z. Jian-

Yong and Z. Yong-Sheng, "Lagrange multiplier method used in BESIII kinematic fitting", *Chinese Physics C*, Vol. 34, No. 2, p. 204, 2010, http://stacks.iop.org/1674-1137/34/i=2/a=009.

23. Jadach, S., *KKMC Event Generator Web Page*, 2000, http://jadach.web.cern.ch/jadach/KKindex.html, March 2015.

24. Amsler *et al.*, "Review of Particle Physics", *Physical Review B*, Vol. 667, 2008.

25. Collaboration, B., *BESIII Event Generator*, 2015, http://docbes3.ihep.ac.cn/DocDB/0000/000018/001/guide.pdf, March 2015.

26. Ryd, A., D. Lange, N. Kuznetsova, S. Versille, M. Rotondo *et al.*, "EvtGen: A Monte Carlo Generator for B-Physics", *BABAR Analysis Document*, 2005.